Proc. of SPIE Vol. 1780, Lens and Optical Systems Design, ed. H Zuegge (Apr 1993) Copyright SPIE

THEORETICAL ANALYSIS OF OPTICAL SYSTEMS SUBJECTED TO MECHANICAL STRESS. AN APPLICATION TO I.S.O. STAR SENSOR DESIGN

S.Pieri, A.Romoli - A.Landi, P.Sampaoli
OFFICINE GALILEO S.p.A. - Via Einstein 35, Campi Bisenzio
50013, FIRENZE, ITALY - tel:++39.55.8950, fax:++39.55.8950611

ABSTRACT

This work concerns the analysis of errors induced on optical systems by mechanical stresses. These errors are consequence of deformations induced by mounts, spacers and similar, in contact with the optical surfaces.
This analysis is essential to drive the mechanical design of very accurate optomechanical systems. The authors developed a method based on a finite elements modelling of the optical system and on interferometric measurement of the real surfaces deformation.
The mechanical behaviour of opto-mechanical items is evaluated by means of a structural analysis software package (ANSYS).
The deformed finite elements model is transformed in a surface representation suitable for optical ray tracing, by means of a Zernike polynomial fitting.
The mechanical stresses of real optical elements are measured by an interferometer and the surfaces are represented fitting the reflected or transmitted wavefront with the same method.
The complete optical system under stress condition is then analyzed using an optical design program provided of a specialized ray tracing routine, supporting a Zernike polynomial representation of optical surfaces.
An application of this method was done on the opto-mechanical design of I.S.O. Star Sensor developed within an ESA program.

1. Fundaments

The method described in this paper is very useful to foresee the optical quality of mechanically stressed optical systems.
Stresses can be induced on optical elements by mechanical parts.

Thermal expansion differences between mounts and optical elements, pressure differences, or boundary forces applied to the items to hold them, and so on, can cause deformation of effective optical surfaces. If the stress applied to an optical element is very strong, it should involve other phenomena, as birifringence, but these aspects are not examined in this paper.

It is possible, by means of existing codes, to analize this kind of deformations of an optical item. Structural analysis codes, generally, operate on a discrete data base, made of a regular set of points. In this way optical surfaces of the item, should be approximated by a set of flat facetes.
But this approach to describe optical surfaces is unsuitable for optical image quality analysis. Indeed, finite ray tracing technique requires to know

exactly both incidence point and the corresponding surface normal. The rough approximation, in which any surface is represented by a set of flat facetes, does'nt offer enough precision in order to describe ray paths.
A suitable representation of optical surfaces is made by means of continous, analitically described functions, allowing to compute both incidence point and surface normal, with very high precision.
While data transfer from an optical design data base to a structural analysis code needs no particular elaborations, the reverse operation is more complicated. Indeed the surfaces normally used by the optical designer to set up and optimize an optical system are planes, sferes, asferical surfaces with conical or higher order (normally up to ten) sections, showing rotational symmetry or ellipsoidal transverse section, or toroidal ones.
Transfer of surface shape information to a discrete set of points, suitable for structural analysis programs, involves only evaluation of these functions on a predefined set of points.
But if the item is mechanically stressed, its surfaces shall change their shape, so that they can't be described by the above mentioned analytical expressions.
The reverse transfer problem, from structural analysis data base to the optical design one, can be adequately solved only by fitting the new set of points coordinates using a set of continous functions, able to represent not symmetrical surfaces, allowing to compute coordinates and normal in any, "a priori" unknown, incidence point.

2. Polynomial fitting of optical surfaces

The polynomial fitting used in the method is made by means of a set of Zernike polynomials [Ref.3,4] which are orthonormal on a discrete set of points defined on a circular domain whose radius is one [ref.1], following a procedure indicateded by Frenier and based on the Graam-Schmidt orthogonalization method [ref.2].
The fitting procedure allows to fit a set of Ns samples of a surface Zs(Xs,Ys) defined on Ns points Ps = Xs,Ys encircled in a normalized circular domain by computing N coefficients Bj.
Bj are the weight coefficients of the N preselected Zernike polynomials. The fitting function F(X,Y) is defined on the same circular domain having radius normalized to 1, and is expressed as a linear combination of the Zernike polinomials Vj(X,Y):

$$(1) \qquad F(X,Y) = \sum_{j} Bj\ Vj(X,Y) \qquad ;\ j = 0,1,\ldots,N$$

the computation of the weights Bj is based on a last square procedure which minimizes the mean square difference E between F(Xs,Ys) and the samples Zs(Xs,Ys):

$$(2) \qquad E = \sum_{s=1}^{Ns} [F(Xs,Ys) - Zs(Xs,Ys)]^2$$

These N polinomyals were selected setting N to 36, following the convention used by the most commercially allovable digital phase-shifting interferometers and fringe analysis codes [ref.5,7].
During the study it was developed a software interface capable to convert data base created by the optical design software package PROGET (*) into an appropriate form suitable for the structural analysis code ANSYS(**), and viceversa.
The PROGET to ANSYS conversion is solved computing the coordinates of a predefined set of Ns points Ps on each optical surface which has to be transferred.
That is done using the typical analytical functions S(X,Y) defining the optical surface in the optical design code.
The resulting set of surface points Ps = (Xs,Ys,Zs) is then analyzed, togheter with loads, constraints and other information by the structural analysis code.
The result of the structural computation is a new set of points coordinates Ps' = (Xs',Ys',Zs') ⇒ Zs'(Xs',Ys').
This new set cannot match, in general, with the starting analytical expressions, because the new shape requires more complex mathematical expressions.

The fitting solution is a new function S'(X,Y), achieved by addition of S(X,Y) and F(X,Y):

$$S'(X,Y) = S(X,Y) + F(X,Y) \tag{3}$$

In order to compute the Bj coefficients set, the difference

$$Dz(Xs',Ys') = Zs'(Xs',Ys') - S(Xs',Ys') \tag{4}$$

is evaluated for all the modified points.

This difference Dz(Xs',Ys') has to be fitted by means of (1).

In such a way, the new surface expression S'(X,Y) will be:

$$S'(X,Y) = S(X,Y) + F(X,Y) = S(X,Y) + \sum_{j} Bj\ Vj(X,Y) \tag{5}$$

3. Surface distortion evaluation using measured OPD

A further development allows to measure the effective wave front deformations generated in a stressed optical element by means of an interferometer and to evaluate the corresponding deformation of an optical surface, which causes the same wavefront aberration.

(*) PROGET is a proprietary optical design software package developed by Optical Design Department of Officine Galileo S.p.A

(**) ANSYS is a registered code name of Swanson Analysis System Inc.

Interferometrical tests of optical elements has to be made in self-collimating condition of the measuring beam on the selected surface of the optical element.

In order to convert a wavefront error E(x,y) into the, corresponding surface distortion, it has to be considered that:

(6) $$E(x,y) = (n - n') [S'(x,y) - S(x,y)]$$

$$= 2 n [S'(x,y) - S(x,y)]$$

where $n = - n'$ is the refractive index of the material in the reflecting space.

So the shape error dS(x,y) results:

(7) $$dS(x,y) = E(x,y)/ 2n$$

The wavefront error E(x,y) can be fitted by means of (1) on a set of Ns points Pi(Xi,Yi):

(8) $$E(x,y) = \sum_{j} Bj\ Vj(x,y) \qquad j = 0, 1,...., N$$

The fitting (8) is generally done by the software of the interferometer, and thus it is possible to fit the surface error by means of the expansion:

(9) $$dS(x,y) = \sum_{j} Cj\ Vj(x,y) \qquad j = 0, 1,...., N$$

whose coefficients Cj are computed from Bj, by division by the conversion factor 2n:

(10) $$Cj = Bj / 2n \qquad j = 0, 1,...., N$$

The shape error dS is oriented as the surface normal, and, if the surface aperture isn't too large, it can be assumed:

$$dS = Dz$$

and the fitting can be used directly (see (4) and (5)).

It has to be remarked that this method can be also applied to a refractive surface in an interferometrical set up including more optical elements, provided that the surface is parallel to the interferometric wavefront and the undistorted wavefront shape is known.

4. Optical ray tracing

In order to achieve the purpose to evaluate the image quality of optical systems, it is necessary to solve the basical finite ray tracing problem for surfaces represented by (5).
The most general position of a ray trace problem, is that to individuate incidence point coordinates Pi = (Xi,Yi,Zi) on the effective optical surface, for a given ray (defined by three coordinates Xo, Yo, Zo, and by its direction) and to compute the emerging ray direction by means of the knowledge of the surface normal and of the law of optical deviation (refraction, reflection and so on).

The unit vector:

$$(11) \qquad \underline{U} = Ux\,\underline{i} + Uy\,\underline{j} + Uz\,\underline{k} \qquad (Ux^2 + Uy^2 + Uz^2) = 1$$

individuates the initial direction of the ray, and the unit vector $\underline{N}$:

$$(12) \qquad \underline{N} = Nx\,\underline{i} + Ny\,\underline{j} + Nz\,\underline{k} \qquad (Nx^2 + Ny^2 + Nz^2) = 1$$

individuates the surface normal.

The first task, to find the incidence point, can be solved by means of a recursive method, starting from the intersection between the ray and the second order approximated expression of the surface S'(X,Y).
That means all terms with degree higher than 2 are neglected, in first approximation.

The approximate position knowledge of Pi = Xi, Yi, Zi on the ray, allows to evaluate the effective value , on the surface at the coordinates Xi, Yi of S'(Xi, Yi), starting from eq.(5):

$$(13) \qquad S'(Xi, Yi) = S(Xi, Yi) + F(Xi, Yi) =$$

$$= S(Xi, Yi) + \sum Bj\ Vj(Xi, Yi)$$

From the same function is possible to compute the gradient function $\nabla g(X,Y,Z)$, being:

$$(14) \qquad g(X,Y,Z) = S'(X,Y) - Z$$

$$(15) \qquad \nabla g = \frac{\partial g}{\partial x}\,\underline{i} + \frac{\partial g}{\partial y}\,\underline{j} + \frac{\partial g}{\partial z}\,\underline{k}$$

The surface normal unit vector $\underline{N}$ at the point (Xi, Yi) is given by:

$$(16) \qquad \underline{N}\,(Xi, Yi) = \frac{\nabla g}{|\,\nabla g\,|}$$

that allows to determine ray intersection with the plane tangent to the surface, determining another point P'(Xi',Yi') closer to the solution. The recursive application of these formulas is made until the distance between P and P' is lower than a prefixed small quantity.
It has been necessary to develope gradient formulas for Zernike polynomials, in order to know the surface normal.

This is possible knowing the form of each polynomial gradient:

$$\nabla V_j(X,Y) \qquad j = 0, 1, \ldots, N \tag{17}$$

Indeed:

$$\nabla g(X,Y,Z) = \nabla \left[S(X,Y) + \sum B_j V_j(X,Y) - Z \right] = \tag{18}$$

$$= \nabla S(X,Y) + \sum \nabla B_j V_j(X,Y) - \nabla Z =$$

$$= \nabla \left[S(X,Y) - Z \right] + \sum B_j \nabla V_j(X,Y)$$

In terms of normal unit vectors this can be resumed writing:

$$\underline{N}'(Xi,Yi) = \frac{\underline{N}(Xi,Yi) + \sum B_j \underline{N}_j(Xi,Yi)}{\left| \underline{N}(Xi,Yi) + \sum B_j \underline{N}_j(Xi,Yi) \right|} \tag{19}$$

where $\underline{N}_j(Xi,Yi)$ are the unit vectors normal to the Zernike surfaces $Z = V_j(X,Y)$.

These vectors are found developing polar gradient expressions for each Zernike polynomial polar expression, and converting them in their cartesian expressions. The above described algorythms were developed in form of computer routines, allowing to simulate ray tracing through stressed optical surfaces.

5. Experimental results

The first application of the method was made on I.S.O. star sensor objective, which is shown in fig.1.

The criticality in mounting this catadioptric objective, which has to be subjected to the strong launch conditions, needed to investigate alternative way to bound the Mangin primary mirror, the optical element most sensitive to the boundaries condition.

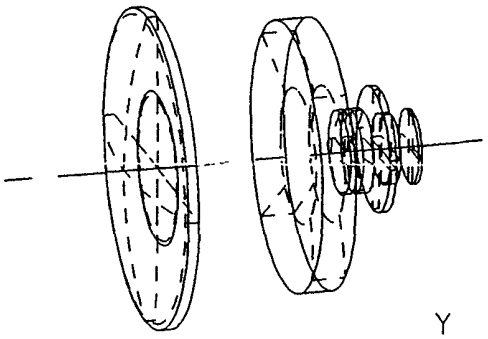

Fig.1 - Optical layout of I.S.O. star sensor catadioptric objective.

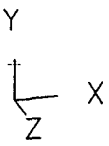

Fig.2 - Mangin mirror: a) Finite element model produced by ANSYS; b) distortion was simulated with the structural analysis code.

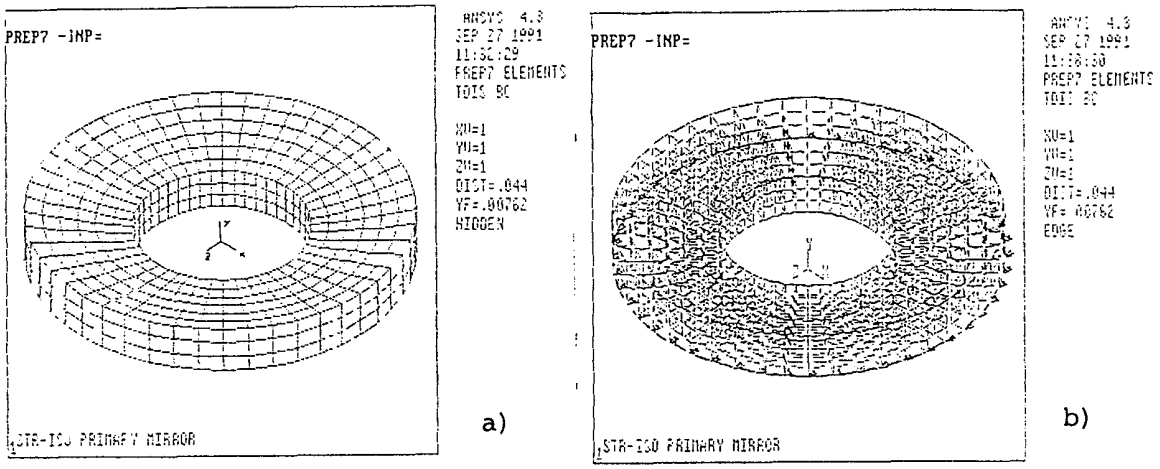

The mechanical approach provided to use two kinds of retaining ring to block the mirror against its seat on the barrel:
One type was rigid, simply screwed and tightened on the mirror surface. The other was elastic, also made of a screwed ring, but provided of a flexible part, in order to uniformely distribute the load onto the mirror edge.
This second type of ring was conceived in order to control the effective load on the mirror and assembly repeatability.
The ring should have to be screwed in the barrell, pushing on the refractive surface of the Mangin mirror, and the load of the ring had to be balanced, just only to satisfy the launch requirements, by measuring the flexible ring shortening.
In both cases the seat on the barrel was conceived conical, in order to be tangent to the rear reflecting surface of the primary mirror.

A structural analysis was done in order to evaluate the elastic solution. It was assumed a manufacturing error of the seat, so that the mirror rear surface had only three contact points on its seat (each placed 120° from the others).
The distortion of the reflecting surface, in consequence of ring load, has been computed, and the distorted surface shape was fitted following the method described in section 1. The fitting was used as shape data of the surfaces in order to compute the Mangin mirror wavefront error and related interferogram, on unit magnification condition, by means of finite ray tracing, as described in section 4.

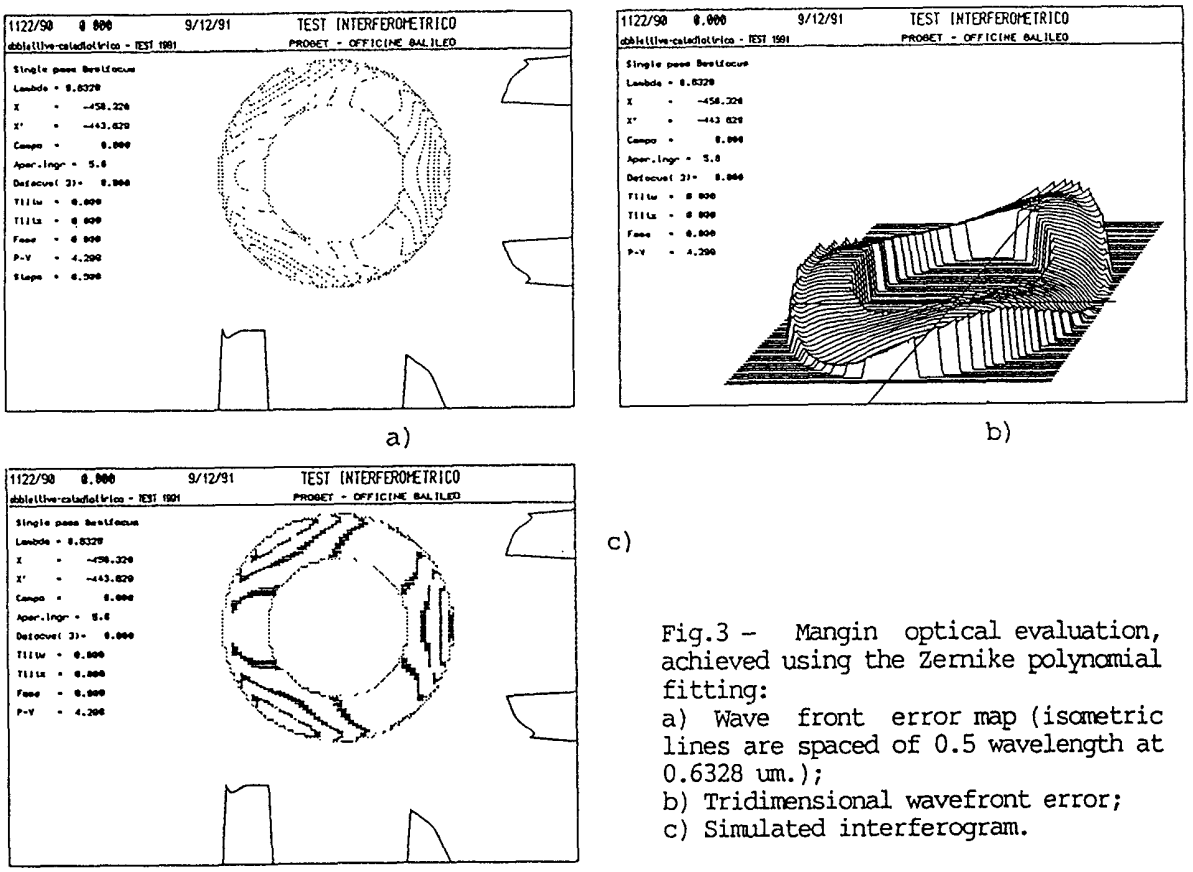

Fig.3 - Mangin optical evaluation, achieved using the Zernike polynomial fitting:
a) Wave front error map (isometric lines are spaced of 0.5 wavelength at 0.6328 um.);
b) Tridimensional wavefront error;
c) Simulated interferogram.

Fig.3 concerns the results of these computations: fig.3a) shows the wavefront error in the best focus, dotted lines representing isometric levels in steps of 0.5 wavelenght (0.6328 um); fig.3b) shows 3-dimensional wavefront error, and fig.3c) shows the simulation of the corresponding interferogram.

The complete optical system was set up, including the distorted Mangin surfaces, and optical quality analysis was carried out, and the results are shown in fig.4. The wavefront error of the objective, at the wavelenght of 0.6328 micrometers, is shown in fig.4a), while the simulated single pass interferogram is shown in fig.4b).
The objective polichromatic diffractive tangential (continous line) and sagittal (dashed line) Line Spread Functions on axis are shown in fig.5a), while the polychromatic Diffractional Point Spread Function is shown in 5c).
The tangential and sagittal Centroid Error Functions are shown in 5b). The spot diagrams in fig.5d) are done for the five wavelenghts of the spectral band of the spectral response curve displayed on the left side of this picture. It can be remarked, as it could be reasonably foreseen, the presence of trilobate astigmatism in all the pictures, both on the mirror and on the objective.

The analisys was supported by a physical set up. The real mirror and mechanical seat appear to match only in two points instead of three.
The experimental interferogram of the Mangin mirror is shown in fig.6a).

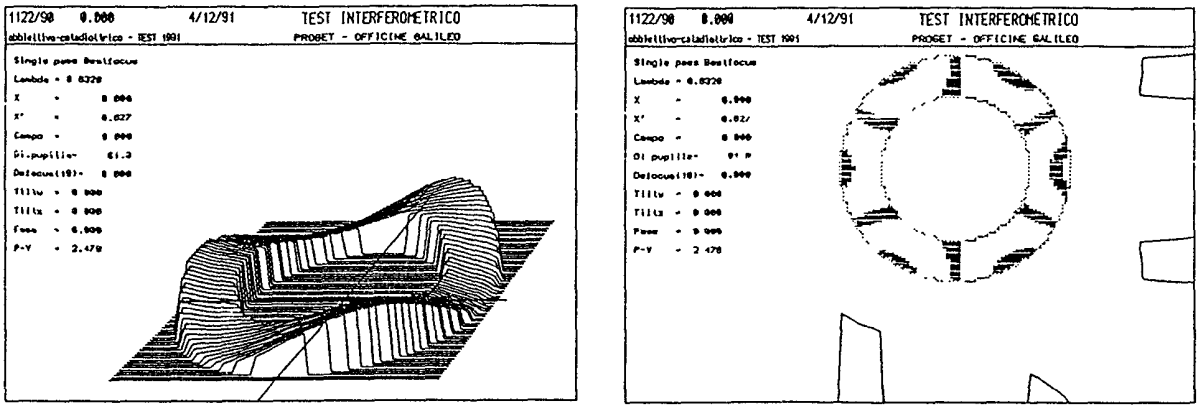

a) b)

Fig.4 – I.S.O. objective computed optical quality. Distortion of the mirror surfaces was taken into account: a) Tridimensional wavefront error; b) Simulated single pass interferogram.

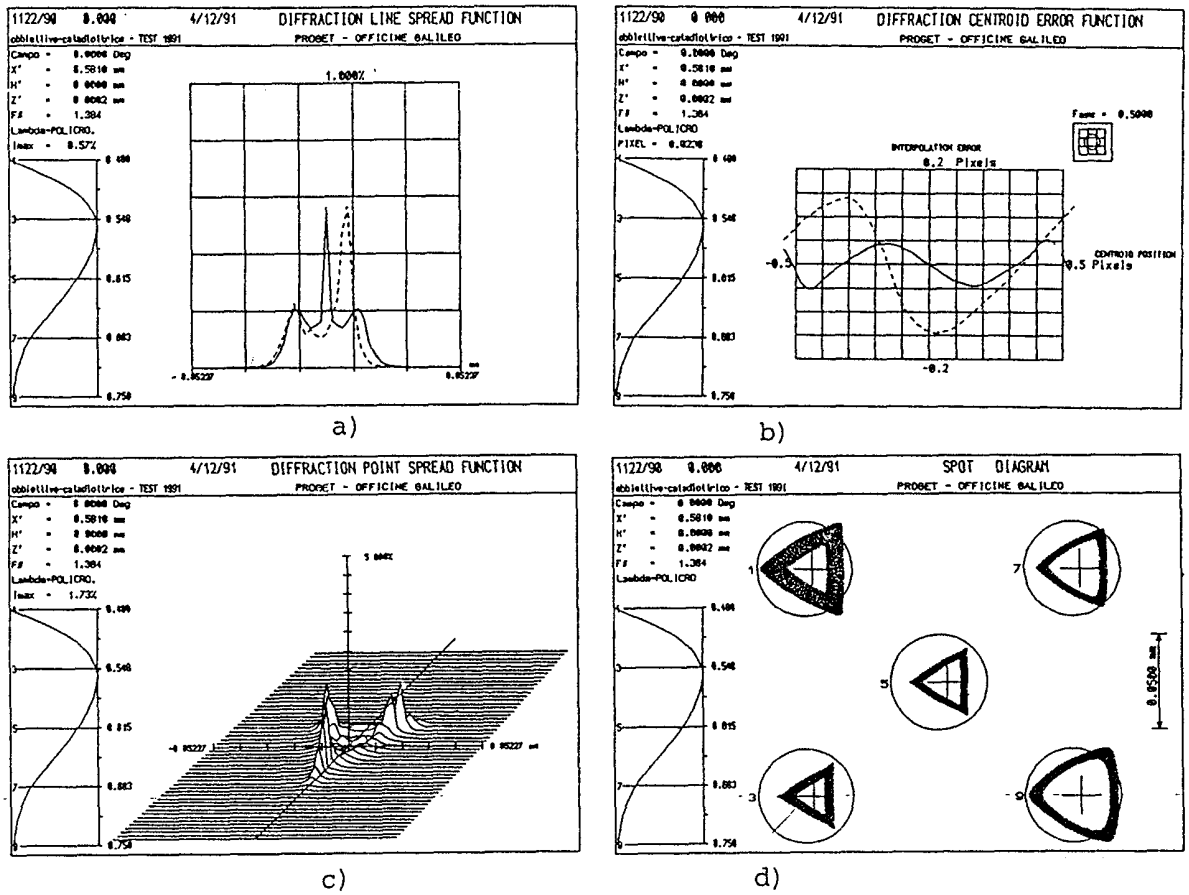

a) b)

c) d)

Fig.5 – I.S.O. objective computed polychromatic optical quality, according to the spectral efficiency curve on the left: a) Axial tangential (continous line) and sagittal (dashed line) L.S.F.; b) Axial C.E.F.; c) Axial P.S.F.; d) Axial spot diagrams at five wavelenghts of the chromatic band.

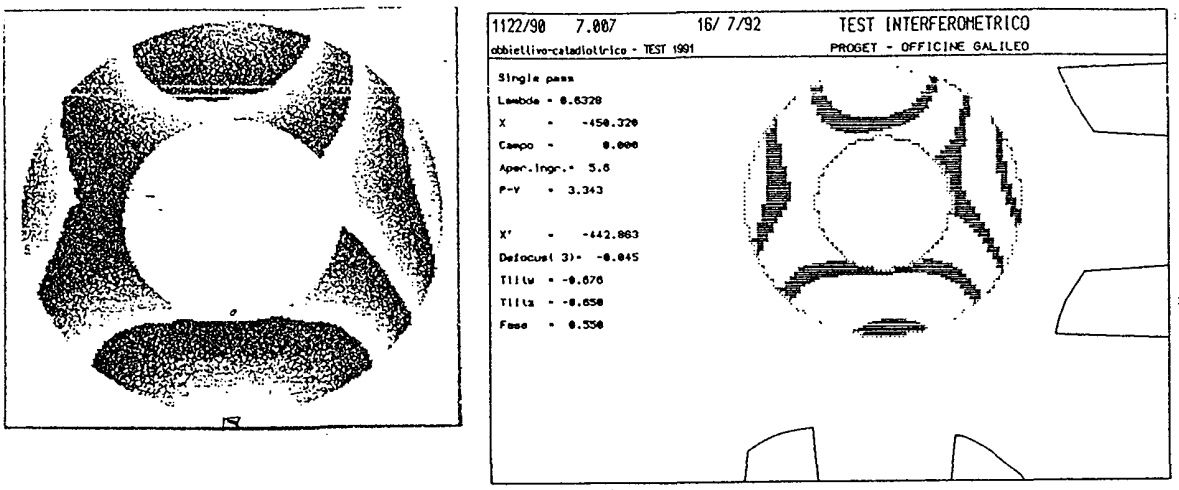

a) b)

Fig.6 – a) Mangin mirror experimental interferogram; b) Computed interferogram, starting from the fitting of experimental data of a).

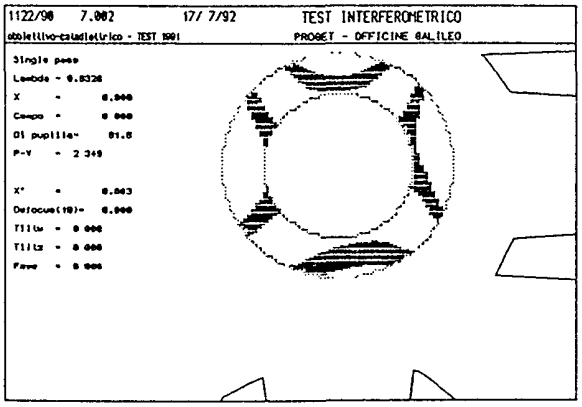

a)

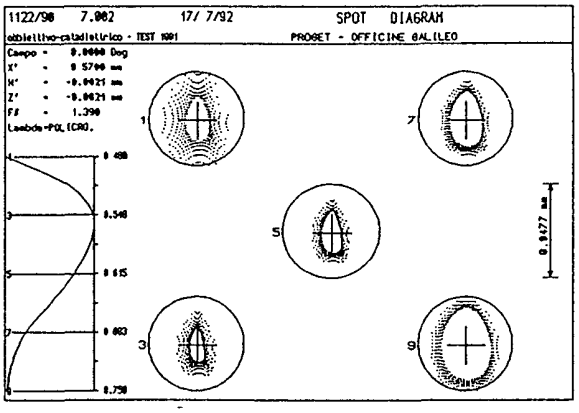

b)

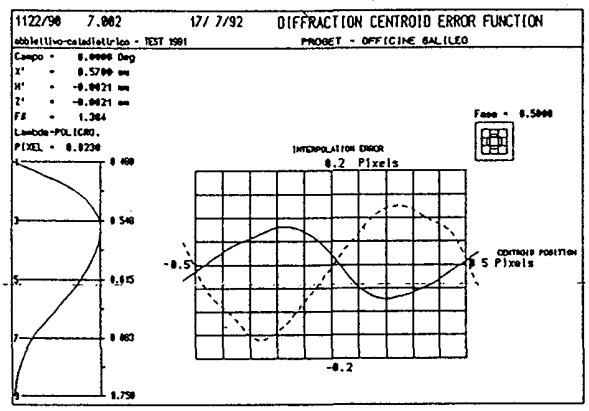

c)

Fig.7 – The objective computed image quality, starting from measured data of the Mangin mirror:
a) interferogram;
b) axial spot diagrams;
c) Polychromatic C.E.F.

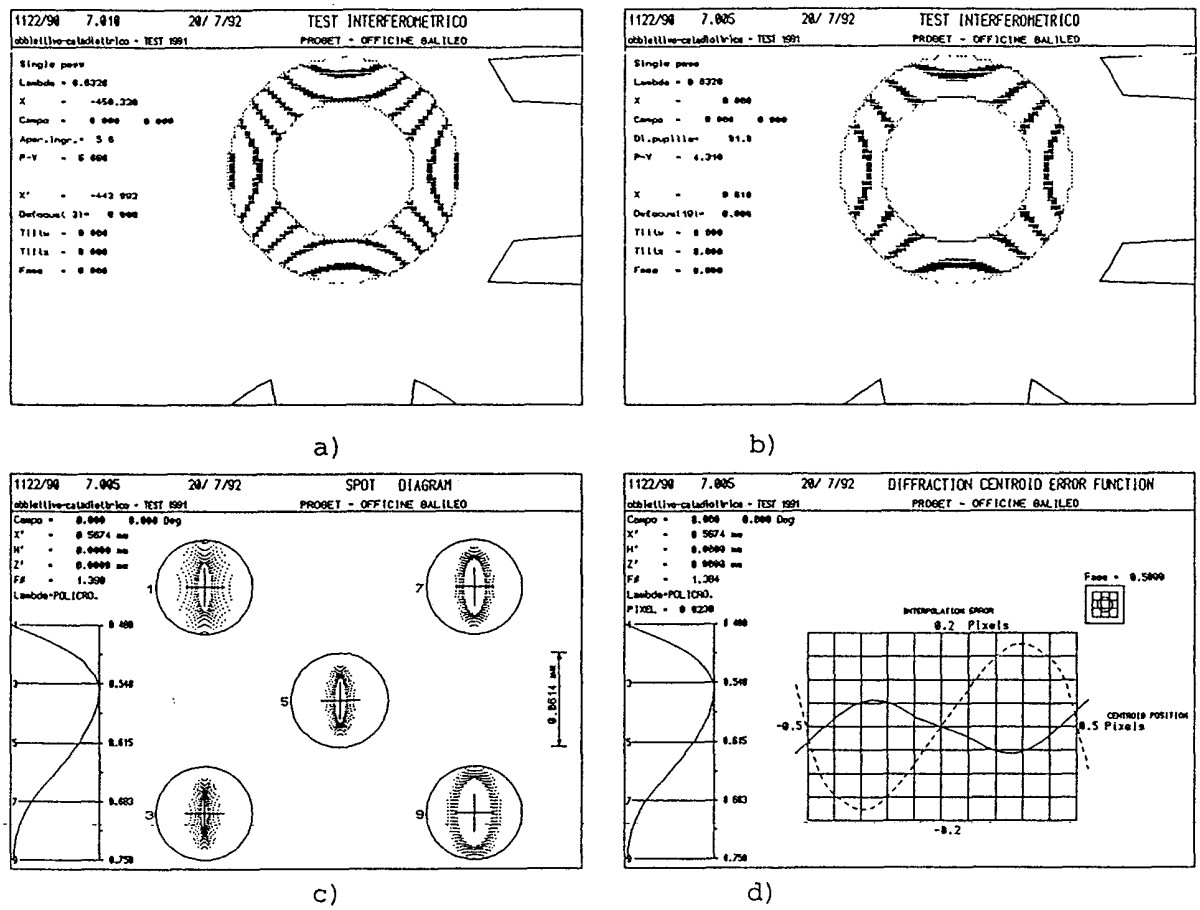

Fig.8 – Quality evaluation starting from ANSYS modellation and simulation: a) Computed Mangin interferogram; b) computed single pass interferogram of the complete objective; c) spot diagrams; d) C.E.F.

The corresponding wavefront error was fitted by means of Zernike polinomials finding the Bj coefficients of (8), and by applying (10) a surface distortion was attributed to the reflecting surface, assuming that the error contribution of the refractive surface is negligeable. The computed interferogram of the Mangin mirror, achieved as described in section 3. and 4. is shown in fig 6.b).
Fig. 7.a), b) and c) show the image quality for the complete objective.

There is remarkably good agreement between computed and experimental interferogram.
This interferogram points out a considerable amount of normal and not trilobate astigmatism.
It was assumed that the Mangin's reflecting surface could have only two opposite contact points on its mechanical seat, rather than three, as previously foreseen; that is because the highest manufacturing error of the conic seat on the barrel is ovaling.

A new simulation of this hypotesys was carried out, by means of the structural analysis code. The new surface data were fitted and a new optical analysis was done.

Fig.8 shows in a) the simulated interferogram of the Mangin mirror. It is clear the presence of saddle astigmatism, as it was provided by the structural analysis code.
The difference between the computed interferogram, achieved starting from ANSYS, and the experimental one is caused by a mismatch between computed and real loads due to a wrong extimation of the elastic ring stiffness.

Fig.8.b), shows the simulated interferogram of the objective with the distorted mirror.

The polychromatic effects of this astigmatism in the objective are pointed out in fig.8, in c) and d).

It was clear that this way to bind the mirror had no future, unless the shape errors on the mechanical seat should be negligeable, compared with the optical tolerances of the mirror: that means, in other words, that the shape of the mechanical seat has to copy very well that of the optical surface. That is possible to do only by optical lapping of the mechanical seat.
One can reverse the sense of this last argument, stating that, with an elastic retaining ring, the Mangin mirror reflecting surface copies the seat shape and its possible distortion.
The result is a higher sensitivity to the barrel distortions. As a consequence, the elastic approach was rejected.

The selected solution was that with the rigid retaining ring, but with some improvements from the starting idea. The rear seat on the barrel was lapped, in order to reduce the conctact uncertainity with the mirror surface. In this way, shaking the system while screwing the ring, it is possible to eliminate the air gap between optics and retainers. That way requires very low load to avoid the mirror moves during the launch. The screw couple is used to check the process of assembling, instead of the load.

6. Acknowledgments

The authors wish thank Monica Olivieri of Officine Galileo Optical Design department for her kind cooperation in analizing I.S.O. objective performances.

REFERENCES

[Ref.1] E.R.Freniere, O.E.Toler, R.Racer: "Interferogram evaluation program for the HP-9825A calculator"; Optical Engineering 20(2), 253-255 (March/April 1981).
[Ref.2] G.E.Forsythe: "Generation and use of orthogonal polynomials for data fitting on a digital computer"; J.Soc.Ind.Appl.Math., 5, 74 (1957).
[Ref.3] M.Born and E.Wolf: "Principles of optics"; Pergamon Press, 1964.
[Ref.4] D.Malacara: "Optical Shop Testing"; John Wiley & Sons, 1978.
[Ref.5] Zygo Digital Interferometer Handbook.
[Ref.6] Moeller and Wedel Digital Phase Shift Interferometer Handbook.
[Ref.7] Wyko Digital Phase Shift interferometer Handbook.